

## **Sequential anaerobic and electro-Fenton processes mediated by W and Mo oxides for degradation/mineralization of azo dye methyl orange in photo assisted microbial fuel cells — Source link**

Qiang Wang, Liping Huang, Xie Quan, Gianluca Li Puma


**Institutions:** Dalian University of Technology, Loughborough University

**Published on:** 15 May 2019 - Applied Catalysis B-environmental (Elsevier)

**Topics:** Partial oxidation, Mineralization (soil science) and Redox

Related papers:

- [Intensified degradation and mineralization of antibiotic metronidazole in photo-assisted microbial fuel cells with Mo-W catalytic cathodes under anaerobic or aerobic conditions in the presence of Fe\(III\)](#)
- [Enhancement of azo dye degradation and power generation in a photoelectrocatalytic microbial fuel cell by simple cathodic reduction on titania nanotube arrays electrode](#)
- [Electrosynthesis of acetate from inorganic carbon \(HCO<sub>3</sub><sup>-</sup>\) with simultaneous hydrogen production and Cd\(II\) removal in multifunctional microbial electrosynthesis systems \(MES\)](#)
- [Microbial Fuel Cells: Methodology and Technology†](#)
- [A new clean approach for production of cobalt dihydroxide from aqueous Co\(II\) using oxygen-reducing biocathode microbial fuel cells](#)

Share this paper:    

View more about this paper here: <https://typeset.io/papers/sequential-anaerobic-and-electro-fenton-processes-mediated-3w0ww4kfc7>

January 4, 2019 R2

Submitted to *Appl Catal B: Environ*

Special issue - Honoring Cesar Pulgarin (LACWWT)

**Sequential anaerobic and electro-Fenton processes mediated by W and Mo oxides for degradation/mineralization of azo dye methyl orange in photo assisted microbial fuel cells**

Qiang Wang<sup>1</sup>, Liping Huang<sup>1,\*</sup>, Xie Quan<sup>1</sup>, Gianluca Li Puma<sup>2,\*</sup>

1. Key Laboratory of Industrial Ecology and Environmental Engineering, Ministry of Education (MOE), School of Environmental Science and Technology, Dalian University of Technology, Dalian 116024, China

2. Environmental Nanocatalysis & Photoreaction Engineering, Department of Chemical Engineering, Loughborough University, Loughborough LE11 3TU, United Kingdom

**Corresponding authors:**

(Huang L.) [lipinghuang@dlut.edu.cn](mailto:lipinghuang@dlut.edu.cn)

(Li Puma G.) [g.lipuma@lboro.ac.uk](mailto:g.lipuma@lboro.ac.uk)

The authors declare no competing financial interest.

## Abstract

The intensification of the degradation and mineralization of the azo dye methyl orange (MO) in contaminated water with simultaneous production of renewable electrical energy was achieved in photo-assisted microbial fuel cells (MFCs) operated sequentially under anaerobic - aerobic processes, in the presence of Fe(III) and W and Mo oxides catalytic species. In this novel process, the W and Mo oxides deposited on the graphite felt cathodes accelerated electron transfer and the reductive decolorization of MO. Simultaneously, the mineralization of MO and intermediate products was intensified by the production of hydroxyl radicals (HO•) produced by (i) the photoreduction of Fe(III) to Fe(II), and by (ii) the reaction of the photochemically and electrochemically produced Fe(II) with hydrogen peroxide, which was produced in-situ during the aerobic stage. Under anaerobic conditions, the reductive decolorization of MO was driven by cathodic electrons, while the partial oxidation of the intermediates proceeded through holes oxidation, producing N,N-dimethyl-p-phenylenediamine. In contrast, under aerobic conditions superoxide radicals ( $O_2^{\bullet-}$ ) were predominant to HO•, forming 4-hydroxy-N,N-dimethylaniline. In the presence of Fe(III) and under aerobic conditions, the oxidation of the intermediate products driven by HO• superseded that of  $O_2^{\bullet-}$ , yielding phenol and amines, via the oxidation of 4-hydroxy-N,N-dimethylaniline and N,N-dimethyl-p-phenylenediamine. These sequential anaerobic and electro-Fenton processes led to the production of benzene and significantly faster oxidation reactions, compared to either the anaerobic or the aerobic operation in the presence of Fe(III). Complete degradation and mineralization ( $96.8 \pm 3.5\%$ ) of MO (20 mg/L) with simultaneous electricity production (0.0002 kWh/kg MO) was therefore achieved with sequential anaerobic (20 min) - aerobic (100 min) operation in the presence of Fe(III) (10 mg/L). This study demonstrates an alternative and environmentally benign approach for efficient

remediation of azo dye contaminated water with simultaneous production of renewable energy.

**Keywords:** photo-assisted microbial fuel cells; azo dye; electro-Fenton; mineralization; decolorization

## 1. Introduction

Azo dyes account for 70 – 80% of the annual global dyes production. Approximately 10 – 15% of these dyes are discharged into surface water bodies, causing significant environmental problems associated with their high color and high chemical oxygen demand (COD), and threats to human health due to the carcinogenicity and teratogenicity of their breakdown products [1-3].

A range of treatment methods have been proposed for the treatment of azo dye wastewaters including physical, biological, advanced oxidation and electrochemical processes [1,3-5]. However, the high operating cost associated with these methods, incomplete azo dye degradation, secondary pollution and high energy consumption, require the development of more environmental friendly and cost-effective strategies for the treatment of azo dye wastewaters.

Photo-assisted microbial fuel cells (MFCs) have recently emerged as a promising alternative method for simultaneous azo dyes degradation and electricity generation [6-8]. In these systems, the oxidation of organic wastes at the anode extracts electrons, which are then transferred through an external circuit to the photocatalytically active cathode, where the cleavage of the azo double bond occurs (reductive dye decolorization). For this purpose, rutile-coated graphite [9] and TiO<sub>2</sub>-coated nickel foam [10] have been proposed as photo-active cathodes in MFCs and other bioelectrochemical systems, for efficient electron transfer to the azo dyes molecules. However, since TiO<sub>2</sub> based photocatalysts mainly respond to the ultraviolet component of the solar radiation spectrum, Pd-modified silicon nanowire or graphite carbon nitride/BiOBr heterojunction have been further developed to widen the cathode response to the visible (up to 43% of the solar radiation) [11,12]. The conduction band potentials of these visible active photocatalysts (less than –0.54 V vs. standard hydrogen electrode, SHE) are lower than the theoretical electrode potential for hydrogen evolution

( $-0.414$  V vs. SHE). Therefore, in these systems the generation of hydrogen further consumes electrons as a side reaction, decreasing the overall rate of azo dyes decolorization [11,12].

In sharp contrast, visible light active W and Mo oxides exhibit a much higher conduction band potential ( $0.40$  V vs. SHE) which may suppress the parasite reaction of hydrogen evolution [13,14]. Thus, the W and Mo oxides deposited on photo-active cathodes may be successful to suppress the production of hydrogen in MFCs, further enhancing the rate of azo dye decolorization and mineralization under visible solar light irradiation. A further enhancement of the rates may also be achieved by an appropriate shift of the operating conditions in the photo-assisted MFCs, from anaerobic to aerobic, due to the critical role played by the operational conditions in azo dye decomposition. In general, azo dyes mineralization is achieved through an easy initial break of the azo double bond and through the subsequent oxidation of the resulting recalcitrant intermediates [15,16]. Anaerobic conditions usually favor the break of the azo double bond, but are unsuitable for the subsequent mineralization of the intermediates [9-11]. Conversely, aerobic conditions favor azo dye mineralization but are disadvantageous for its decolorization [17-20]. Therefore, an appropriate shift of the operating conditions, from anaerobic to aerobic, may be engineered in photo-assisted MFCs to accelerate the initial rupture of the azo dye double bond and also the subsequent efficient mineralization of the recalcitrant intermediate products generated. Indeed, such shift has been successfully employed in the mineralization of azo dyes in MFCs comprising anaerobic bioanodes and aerobic biocathodes [17-20].

Under aerobic conditions, the presence of Fe(III) in MFCs and other bioelectrochemical systems has been proved to create the conditions for electro-Fenton like reactions involved with in-situ produced  $H_2O_2$ , which may further assist the mineralization of azo dyes [21-23]. In addition,

in the presence of light irradiation, the further production of HO• radicals by Fe(III) photoreduction may favor the mineralization of the azo dyes in comparison to conventional Fenton processes [24,25]. Therefore, the addition of Fe(III) under aerobic conditions in photo-assisted MFCs with W and Mo oxides deposited on the cathodes, may lead to a further improvement of the rates of mineralization of azo dyes.

In this study, the decolorization and mineralization of methyl orange (MO) model azo dye was investigated in photo-assisted MFCs comprising W and Mo oxides deposited on graphite felt cathodes irradiated with visible light. The impact of a shift of the operating conditions in the reaction chambers, from anaerobic to aerobic, with simultaneous Fe(III) addition was investigated for increasing the rate of MO decolorization and mineralization. The process parameters, circuit current, linear sweep voltammetry (LSV), cyclic voltammetry (CV) and electrochemical impedance spectroscopy (EIS) were extensively monitored to explain the results observed and the overall performance of the system. The possible MO degradation pathways were established based on analysis of the resulting reaction intermediates obtained during the MO decolorization and mineralization.

## **2. Materials and methods**

### *2.1 Reactor configuration*

Photo-assisted two-chamber MFCs were assembled using two cubic polymethyl methacrylate blocks with an inner cylinder 3 cm in diameter. The two chambers were separated by a cation exchange member (CMI-7000 Membranes International, Glen Rock, NJ). Graphite felt (2.0 cm × 2.0 cm × 0.5 cm, Sanye Co., Beijing, China) anode and cathode electrodes were used due to their suitability for H<sub>2</sub>O<sub>2</sub> production in MFCs [26,27]. The anode was connected to the external circuit

with a carbon rod and the cathode with a titanium wire. A 10  $\Omega$  resistance was used as external load. All materials used were cleaned as previously described [28]. The effective operating volumes of the anode and cathode were 13 mL each. A saturated calomel reference electrode (SCE, 241 mV vs. standard hydrogen electrode (SHE)) was placed in the cathode chamber to monitor the cathode potential, with all voltages reported here vs SHE. The reactor anodes were wrapped in aluminum foil to exclude light irradiation.

The cathode electrode in each MFC was irradiated by a 100 W iodine tungsten lamp emitting radiation in the visible-light wavelength range of 400 – 800 nm, placed in parallel to the electrode at a distance of 15 cm, as shown elsewhere [10]. The incident photon irradiance was 23.3 mW/cm<sup>2</sup>. The lamp was refrigerated by a cool-fan and the MFCs were surrounded in a jacket with a continuous circulation of water to maintain the temperature of the reaction chambers isothermal at 25  $\pm$  3  $^{\circ}$ C.

## *2.2 Anode inoculation and acclimation*

The anodes were inoculated with the effluent collected from separate acetate-fed MFCs, with an equivalent volume of nutrient solution as previously reported [6,8,9,28]. The separate acetate-fed MFCs were previously inoculated with samples collected from a primary sedimentation tank of the Lingshui wastewater treatment plant (Dalian, China) which contained (g/L) total COD, 0.38  $\pm$  0.02; soluble COD, 0.20  $\pm$  0.04; ammonia nitrogen, 0.22  $\pm$  0.08 with pHs 6.6 – 7.2. The anodic medium contained (g/L): sodium acetate 1.0, KH<sub>2</sub>PO<sub>4</sub> 4.4, K<sub>2</sub>HPO<sub>4</sub> 3.4, NH<sub>4</sub>Cl 1.3, KCl 0.78, MgCl<sub>2</sub> 0.2, CaCl<sub>2</sub> 0.0146, NaCl 0.5, trace vitamins and minerals. The catholyte used during the anode acclimation period, was a 50 mM phosphate buffer. Both anolyte and catholyte were replaced daily. An external resistance of 1000  $\Omega$  was used during the exoelectrogen acclimation period, which was suitable for bacterial acclimation and avoided inaccurate assessment for subsequent power



production [28,29]. The anodes were considered fully acclimated when the anode potential stabilized at  $-0.24$  V for at least three successive batch cycles [28,29].

### *2.3 Preparation of W and Mo oxides deposited on graphite felt electrodes*

The W and Mo oxides deposited on graphite felt electrodes were prepared in-situ. Briefly, the catholyte was replaced by a mixture of  $\text{Na}_2\text{WO}_4 \cdot 2\text{H}_2\text{O}$  and  $\text{Na}_2\text{MoO}_4 \cdot 2\text{H}_2\text{O}$  (Tianjin Bodi Chemistry Co., Ltd., analytically pure) with each metal concentration of 200 mg/L [30,31]. The pH of catholyte was set to 1.5 and the MFCs were operated for 6 h with air sparging at a rate of 80 mL/min [27]. The residual W and Mo in solution were measured to calculate the amount of metals loaded onto the graphite felt cathodes (W:  $0.22 \text{ mg/cm}^2$ ; Mo:  $0.28 \text{ mg/cm}^2$ ). The cathodes were then taken out and subsequently calcined at  $450$  °C for 2 h in air to increase their photo response [32]. The light response plot was shown in Fig. S1 in the Supporting Material (SM). The graphite felt cathodes loaded with the W and Mo oxides were finally reassembled back in the photo-assisted MFCs.

### *2.4 Operation of photo-assisted MFCs with graphite felt cathodes loaded with W and Mo oxides*

Typical concentrations of MO in the tested wastewaters largely vary from 5 mg/L to 1000 mg/L [11,21,22,33,34]. Considering that low circuital currents of  $0.1 - 4.0 \text{ A/m}^2$  in MFCs [21,26] are theoretically more suitable for the degradation of lower concentrations of MO, an initial MO of 20 mg/L was appropriately chosen in this study. The photo-assisted MFCs were operated under either fully anaerobic conditions (continuous  $\text{N}_2$  sparging) or fully aerobic conditions (continuous air sparging), both at a rate of 80 mL/min. The initial anaerobic operational period of the cathodic chamber was optimized to 20 min, which achieved the complete decolorization of MO. After this period, aerobic conditions were established with simultaneous Fe(III) addition to create an electro-Fenton like process, which lasted a further 100 min to favor the mineralization of MO. The

experiments were performed with 5, 10 or 15 mg/L Fe(III) in accordance to the typical range used in other electro-Fenton processes [21,26]. LSVs, CVs and EIS were conducted under anaerobic or aerobic conditions to assess electrochemical performance of the MFCs. Under the optimal sequential anaerobic - aerobic conditions and with 10 mg/L Fe(III), system performance over time was investigated at initial pHs of 2.0, 3.0 or 4.0. The stability of system performance was then assessed based on 10 consecutive operational cycles. At the end of each cycle, the leached W and Mo in the catholyte was evaluated.

Scavengers of ammonium oxalate (AO) for holes, isopropanol (IP) for HO• and benzoquinone (BQ) for O<sub>2</sub>•<sup>-</sup>, normally used for exploring the degradation mechanisms of recalcitrant organics in photocatalysis processes [35-36], were added to the catholyte (0.05 mM) to track the reactive species generated during the photo-assisted azo dye mineralization in the MFCs, under either anaerobic or aerobic conditions [37-41].

Three control experiments were executed to monitor the performance of the photo-assisted MFCs. In the first control experiment, the MFCs with W and Mo deposited graphite felt cathodes were run in the absence of light irradiation, to illustrate the impact of light irradiation on MO decolorization and mineralization. In the second control experiment, the photo-assisted MFCs with bare graphite felt cathodes were run to demonstrate the effect of the photo-active W and Mo deposits on the cathode on MO decolorization and mineralization. In the third control experiment, the photo-assisted MFCs with W and Mo deposited graphite felt cathodes were operated under open circuit conditions (OCCs) to reflect the roles of current generation in MO decolorization and mineralization. Three duplicate reactors were used in all experiments. Unless otherwise stated, the initial pH of the catholyte was set at 3.0 since this is favorable for the Fenton reaction [42]. Boric

acid (0.1 M) was used as buffer and the catholyte pH was maintained at 3.0 using 1.0 M HCl during the MFC operations [43]. All reactors were run in fed-batch mode.

### 2.5 Measurements and analyses

The concentrations of MO were quantified by measuring the absorbance at the maximum visible wavelength of  $\lambda_{max} = 465$  nm using an UV-5500 PC spectrophotometer (Shanghai Metash Instruments Co., Ltd., China) [44]. The mineralization process of MO was monitored through the decay of its COD, which better describes than the total organic carbon (TOC) the reactions in the systems and the decay of the total load of pollutants [45,46,47]. The COD in the catholyte was measured by standard methods using potassium permanganate as the oxidant [48]. The Fe(III), and W and Mo ions were determined according to standard methods [48]. The residual H<sub>2</sub>O<sub>2</sub> in effluent was detected using titanyle sulfate spectrophotometric method [27]. pHs were measured using a pH meter (PHS-3C, Leici, Shanghai). Gas chromatography/mass spectrometry (GC/MS, C5975C, Agilent, USA) was used to validate the intermediate products of MO degradation in the effluents. Prior to GC/MS analysis, the sample solutions of 60 mL were extracted with equivalent volume of dichloromethane. The organic phases were dehydrated by MgSO<sub>4</sub> for 24 h and then concentrated. The initial oven temperature (60 °C for 4 min initially) increased at the rate of 4 °C/min to 260 °C. Temperatures were set at 290 °C for injector and 300 °C for detector. Helium was used as carrier gas at a flow rate of 2 mL/min.

A scanning electron microscopy (SEM) (QUANTA450, FEI company, USA) equipped with an energy dispersive X-ray spectroscopy (EDS) (X-MAX 20 mm<sup>2</sup>-50 mm<sup>2</sup>, Oxford Instruments, UK) was used to characterize the morphology of W and Mo deposits, as well as, the elemental composition on the cathodes surface. X-ray diffraction measurements (XRD) (XRD-6000, Shimadzu

LabX, Japan) were used to investigate the crystal form of the W and Mo species deposited on the cathodes.

LSV was conducted at the open circuit potential (OCP) to 0 V using a potentiostat (BioLogic, VSP, France) at a scan rate of 0.1 mV/s. Power production and current densities were normalized to the geometric surface of the cathode ( $\text{mW/m}^2$ ,  $\text{A/m}^2$ ) or based on per kilogram of de-colored MO ( $\text{kWh/kg MO}$ ) [49,50]. CVs were conducted from  $-0.2$  V to  $1.1$  V using a potentiostat (BioLogic, VSP, France) at a scan rate of  $1.0$  mV/s. EIS was carried out at the frequency ranging from  $100$  kHz to  $0.01$  Hz with a sinusoidal perturbation of  $5$  mV in amplitude at the cathodic OCP [51]. Both CVs and EIS were performed in catholyte using the same potentiostat with a three electrode system consisting of a working electrode, a SCE reference electrode ( $241$  mV vs. SHE) and a Pt foil as counter electrode. The equivalent circuit and detailed values of different resistances were obtained through Zsimpwin software and normalized to the projected area of the cathodes.

## 2.6 Calculations

The decolorization of MO was calculated according to Eq. (1). The mineralization degree of MO was characterized by the percentage of COD removal, calculated by Eq. (2) [49,52].

$$\text{Decolorization (\%)} = \frac{C_0 - C_t}{C_0} \times 100\% \quad (1)$$

$$\text{Mineralization (\%)} = \frac{\text{COD}_0 - \text{COD}_t}{\text{COD}_0} \times 100\% \quad (2)$$

where  $C_0$  is the initial MO concentration (mg/L).  $C_t$  is the MO concentration at operational time of  $t$  (mg/L). Similarly,  $\text{COD}_0$  is the COD value before treatment (mg/L).  $\text{COD}_t$  is the value of COD in the catholyte at operational time  $t$  (mg/L).

One-way ANOVA in SPSS 19.0 was used to analyze the differences among the data, and all of

the data indicated significance levels of  $P < 0.05$ .

### **3. Results and discussion**

#### *3.1 Morphology and structure of W and Mo deposits on the graphite felt cathodes*

Compared to the smooth surface of the bare graphite felt cathodes (Fig. S2A), W and Mo agglomerates with a mesh network structure were observed on the surface of the cathodes (Fig. S2C). EDS further confirmed the presence of the W and Mo elements (Fig. S2B and D). The crystal structure of the metal oxide deposits examined by XRD (Fig. S3), evidenced a number of diffraction peaks at 22.9°, 23.6°, 24.4° and 34.9°, ascribed to the (002), (020), (200) and (202) crystal faces of monoclinic  $\text{WO}_3$  [53], and at 27.3° and 38.9° associated with the (021) and (060) crystal faces of orthorhombic  $\text{MoO}_3$  [54]. These results indicated the successful deposition of crystalline W and Mo species on the graphite felt cathodes.

#### *3.2 MO decolorization and mineralization under fully anaerobic conditions*

Under anaerobic conditions and in the presence of light irradiation, the cathodes with W and Mo deposits achieved a MO decolorization of  $93.8 \pm 1.2\%$  after 5 min. This decolorization was 1.6-fold larger than the controls without W and Mo catalysts, 2-fold larger than in the absence of light irradiation and 20.4-fold higher than under OCCs (Fig. 1A). The amount of MO mineralized was  $33.7 \pm 2.7\%$  after 120 min (Fig. 1B), significantly higher than in the control experiments: without W and Mo deposits ( $7.5 \pm 2.6\%$ ), under darkness ( $7.9 \pm 2.7\%$ ), and under OCCs ( $9.4 \pm 2.5\%$ ). These results in concert demonstrated the cooperative roles of W and Mo catalysts, light irradiation, and circuital current in both MO decolorization and its subsequent mineralization.

Complete MO decolorization was observed after 20 min with a rate of 60 mg/L h (Fig. 1A), which is 10.9 fold higher than the decolourization observed at the same pH of 3.0 with the bare

graphite felt cathodes of MFCs (5.5 mg/L h) [7] and 2-order of magnitude higher than at pH 2.4 with the rutile-coated graphite cathodes of MFCs (0.6 mg/L h) [9] and at a more acidic pH of 1.0 in the photo-assisted MFCs using Pd-modified silicon nanowire as cathodes (0.6 mg/L h) [11]. The efficient rate of visible light absorption and higher conduction band potential exerted by the W and Mo catalysts on the cathodes of the photo-assisted MFCs [9,13] may play a key role in the significant rate of MO decolorization observed.

The above results were supported by the higher circuital current observed in the co-presence of light irradiation and W and Mo deposits in comparison to the control experiments (Fig. 1C). The corresponding power productions were 43.4 mW/m<sup>2</sup> (0.0002 kWh/kg MO) in the co-presence of light irradiation, and W and Mo catalysts (Fig. 1D), 39.8 mW/m<sup>2</sup> (0.0001 kWh/kg MO) in the control in the absence of light irradiation, and 20.3 mW/m<sup>2</sup> (0.0001 kWh/kg MO) in the absence of W and Mo catalysts.

### Here Fig. 1

#### *3.3 MO decolorization and mineralization under fully aerobic conditions and in the presence of Fe(III)*

Under fully aerobic conditions and in the presence of W and Mo catalysts and light irradiation, the MO decolorization was of  $87.2 \pm 1.4\%$  (Fig. 2A), appreciably higher than the control experiments in the absence of light irradiation ( $73.5 \pm 1.4\%$ ), and in the absence of W and Mo deposits ( $64.6 \pm 2.3\%$ ), but lower than the values under fully anaerobic conditions (Fig. 1A). The preferential decolorization of MO under anaerobic rather than aerobic conditions was consistent with other reports, where MO was explored for decolorization under anaerobic conditions [21-23]. However, the aerobic conditions favored the mineralization of MO. The amount of MO

mineralization under fully aerobic conditions reached  $43.8 \pm 3.7\%$  (Fig. 2B), that was 1.3 fold higher than under anaerobic conditions, 3-fold higher than the control experiments in the absence of light irradiation, and 2.7-fold higher than in the absence of W and Mo deposits.

In the presence of Fe(III), W and Mo catalysts and light irradiation, the decolorization of MO decreased to  $55.7 \pm 1.1\%$  (Fig. 2A) but the mineralization of MO increased to  $76.8 \pm 3.5\%$  (Fig. 2B), which suggested a faster conversion rate of the reaction intermediates. The role of Fe(III) under light irradiation can be explained by the formation of reduced products of Fe(II) and  $\text{H}_2\text{O}_2$  which can act as a Fenton system to produce  $\text{HO}\cdot$  radicals for enhancing the further degradation of the MO degradation products. In conclusions, light irradiation and W and Mo catalysts favored the decolorization of MO under anaerobic conditions, while the mineralization of MO was favored under aerobic conditions and further enhanced in the presence of Fe(III).

Under fully aerobic conditions and in the presence of W and Mo catalysts, light irradiation and Fe(III), the highest circuital current of  $0.63 \pm 0.04$  mA (Fig. 2C) associated with power production of  $80.9 \text{ mW/m}^2$  (Fig. 2D) ( $0.0005 \text{ kWh/kg MO}$ ) were achieved.

**Here Fig. 2**

### *3.4 CV and EIS analysis*

The W and Mo deposits on the cathodes catalyzed the reduction of MO, which was evidenced by a shift of the MO reduction onset potentials from 0.62 V to a more positive 0.71 V (Fig. S4A). Light irradiation increased the redox peak currents ( $-0.43$  mA at 0.35 V to  $-0.55$  mA at 0.35 V;  $0.63$  mA at 0.78 V to  $0.65$  mA at 0.72 V) (Fig. S4A), indicating the enhanced MO reduction and oxidation by light irradiation, consistent with the kinetics results (Fig. 1A and 1B). In the absence of light irradiation and in the presence of  $\text{O}_2$ , the MO reduction peak current decreased to  $-0.26$  mA at 0.35

V and the MO oxidation peak current increased to 0.65 mA at 0.84 V (Fig. S4A), demonstrating that O<sub>2</sub> decreased the MO reduction but increased its oxidation. Similarly, the co-presence of O<sub>2</sub> and Fe(III) resulted in a further decrease in the reduction peak current and an increase in the oxidation peak current (Fig. S4A). These observations were consistent with the results shown in Fig. 2A and 2B.

The EIS spectra (Fig. S4B) were analyzed by fitting spectra to an equivalent circuit (Fig. S5A and Table S1). In the absence of light irradiation, the resistance of the solution and the electrode loaded with the W and Mo catalysts ( $R_s$ ) equaled 56.7  $\Omega\cdot\text{cm}^2$  and the charge transfer resistance ( $R_{ct}$ ) equaled 22.3  $\Omega\cdot\text{cm}^2$  (Table S1). These results were lower than the corresponding values 74.4  $\Omega\cdot\text{cm}^2$  ( $R_s$ ) and 58.6  $\Omega\cdot\text{cm}^2$  ( $R_{ct}$ ) observed with the bare cathodes in the absence of catalysts. Since the resistance of the solution was the same in the two cases, the decrease of the electrode resistance  $R_s$  in the presence of catalysts should be attributed to the catalytic effect of the metals. The electrode resistance  $R_s$  in the presence of light irradiation decreased to 24.4  $\Omega\cdot\text{cm}^2$  (Table S1), implying that light irradiation might have enhanced the reduction of MO through the decrease in the electrode resistance and through the subsequent increase in the circuital current (Fig. 1C). The charge transfer resistance  $R_{ct}$  in the presence of O<sub>2</sub> increased 143% (Table S1), indicating the unfavorable effect of O<sub>2</sub> for the reduction of MO, in agreement with the results shown in Fig. 2A.

### 3.5 Detection of active reacting species by scavengers

The direct participation of the holes on the cleavage of azo bond of MO was excluded since the rate of MO decolorization, under fully anaerobic conditions, did not change when AO (hole scavenger) was added to the aqueous solution (Fig. 3A and Fig. 1A). This result further confirmed that the decolorization of MO occurred through a reductive rather than an oxidative pathway.



However, the direct involvement of holes was observed for the oxidation of the intermediate products of MO reduction such as sulfanilic acid [7,44], since the presence of AO resulted in an apparent increase in the UV-absorption peak at 248 nm (Fig. 3B) characteristic of sulfanilic acid. The presence of HO• radicals was also excluded since the presence of IP (HO• scavenger) negligibly changed the rate of MO decolorization (Fig. 3A) and the peak height at 248 nm of the reaction intermediate (Fig. 3B), indicating that HO• was not an active species in both MO decolorization and mineralization.

In direct contrast, the dominant active species for the cleavage of azo bond and for the oxidation of the intermediate products, under fully aerobic conditions, was the superoxide radical ( $O_2^{\bullet-}$ ), since strong inhibition of the decolorization of MO ( $69.1 \pm 1.4\%$ , Fig. 3A) and highest peak height at 248 nm (Fig. 3C) were observed in the presence of BQ (superoxide scavenger). The HO• was also a participating species under aerobic conditions, since a slight decrease in MO decolorization (Fig. 3A) and a slight increase in peak height at 248 nm (Fig. 3C) were observed in the presence of IP. However, under fully aerobic conditions and in the presence of Fe(III), the direct participation of HO• was predominant to  $O_2^{\bullet-}$  (the reverse situation found under anaerobic conditions) since the inhibition of MO decolorization (Fig. 3A) and the peak height at 248 nm (Fig. 3D) were more accentuated in the presence of IP rather than BQ. The direct participation of holes under fully aerobic conditions, with or without the presence of Fe(III), was excluded since negligible impact on the rate of MO decolorization (Fig. 3A) and on the peak height at 248 nm (Fig. 3C and 3D) were observed in the presence of AO.

**Here Fig. 3**

### *3.6 Sequential anaerobic and aerobic operation and the impact of Fe(III) dosages on system*

## *performance*

The results presented have shown that higher MO decolorization and negligible mineralization were observed under anaerobic conditions with complete conversion in less than 20 min, while a significantly higher rate of mineralization was observed under fully aerobic conditions, with the addition of Fe(III) further increasing the rate of mineralization. Therefore, the adoption of a sequential operational strategy from anaerobic to aerobic, with simultaneous addition of Fe(III) during the transition phase, should result in the most efficient rates of MO decolorization and mineralization. Fig. 4 shows the results of experiments performed adopting a shift of the operational condition from anaerobic to aerobic after 20 min of operational time with the simultaneous addition of varying doses of Fe(III). The highest rate of MO mineralization and almost complete mineralization after 120 min was observed using 10 mg/L of Fe(III) (Fig. 4A), which should be attributed to the higher rate of HO• production evidenced by the amount of Fe(II) determined in the catholyte (Fig. 4B). It is well known that the reduction of Fe(III) to Fe(II) by photons results in the generation of HO• and the Fe(II) ions from Fe(III) electrochemical reduction react with in-situ produced H<sub>2</sub>O<sub>2</sub> to produce HO• in electro-Fenton process. However, a further increase in Fe(III) (15 mg/L) decreased the mineralization of MO (Fig. 4A), which was ascribed to the simultaneous consumption of HO• by an excessive amount of Fe(II) in the catholyte (Fig. 4B) which acted as a reductive agent [21,55]. The mineralization of MO reached  $96.8 \pm 3.5\%$  (9.7 mg/L h) after 120 min with a sequential operational strategy from anaerobic to aerobic in the presence of an optimized Fe(III) concentration, which was 1.9 times higher than the value observed in the absence of Fe(III) (Fig. 4A), 2.9 times higher than the value observed within an entire anaerobic cycle (Fig. 1B) and 1.3 times higher than the value observed in an entire aerobic cycle (Fig. 2B). The MO mineralization rate

observed under optimized conditions was significantly higher than the 35.2% (5.9 mg/L h) achieved in Fenton systems with 14 mg/L Fe(III) [56], 80.6% (2.9 mg/L h) in Fenton-like systems with g-C<sub>3</sub>N<sub>4</sub>/Ag/γ-FeOOH photocatalyst [57], 57.4% (2.2 mg/L h) in other bioelectrochemical systems at pH of 3.0 with an external applied voltage of 0.7 V [58], and 80.0% (0.6 mg/L h) in conventional photocatalytic processes [59].

#### Here Fig. 4

The MO decolorization with sequential anaerobic to aerobic operational strategy was equivalent to the decolorization achieved in an entire anaerobic cycle (Fig. 1A), and 1.7 times higher than the decolorization achieved under fully aerobic conditions in the presence of Fe(III) (Fig. 2A). These results clearly reflected that a shift from anaerobic to aerobic conditions in MFCs was an efficient approach for both MO decolorization and mineralization. Power productions of 43.4 mW/m<sup>2</sup> during the anaerobic stage (Fig. 1D) and 89.3 mW/m<sup>2</sup> during the aerobic stage (Fig. S6) (0.0002 kWh/kg MO) were simultaneously achieved in this sequential anaerobic (20 min) - aerobic (100 min) operation and Fe(III) (10 mg/L) addition. The residual concentration of H<sub>2</sub>O<sub>2</sub> in the effluent under sequential anaerobic- aerobic conditions and in the presence of 10 mg/L Fe(III) was 1.7 ± 0.4 mg/L, appreciably lower than the concentrations of 10 – 160 mg/L influencing the growth activities of many microorganisms [60,61].

#### 3.7 Reaction intermediate products

The reaction intermediate products formed during the cathodic degradation of MO depended on the operational conditions. Anaerobic operation of the cell led to the formation of N,N-dimethyl-p-phenylenediamine (m/z = 136) (Fig. 5A), which was resulted from the cleavage of

the azo group N=N of MO by electron attack. The same intermediate product was detected during anaerobic decolorization of MO by *Shewanella oneidensis* MR-1 [62]. The undetectable 4-aminobenzenesulfonic acid as one MO reduction product was mainly ascribed to its boiling point exceeding the temperature limit of the GC-MS [62].

In contrast, aerobic conditions led to the appearance of 4-hydroxy-N,N-dimethylaniline ( $m/z = 137$ ) (Fig. 5B), which was resulted from the rupture of the azo bonds of MO by superoxide and HO• oxidation [63]. Aerobic conditions in the presence of Fe(III) resulted in the formation of phenol ( $m/z = 94$ ) and amine ( $m/z = 93$ ) (Fig. 5C), which could be the products of further oxidation of 4-hydroxy-N,N-dimethylaniline and N,N-dimethyl-p-phenylenediamine [64]. The MO decolorization with sequential anaerobic to aerobic conditions and the addition of Fe(III) at the start of the aerobic phase resulted in the formation of benzene ( $m/z = 78$ ) (Fig. 5D), which could be the oxidation product of benzene sulfonic acid derived from 4-aminobenzenesulfonic acid [64]. The undetectable N,N-dimethyl-p-phenylenediamine transformation product under sequential anaerobic to aerobic conditions with Fe(III) addition demonstrated the more efficient oxidation of MO intermediates than either the fully anaerobic or aerobic conditions with accumulated N,N-dimethyl-p-phenylenediamine (Fig. 5A and 5B). Fig. S7 shows the proposed reaction scheme of MO degradation in the photo-assisted MFCs with W and Mo deposited cathodes under a sequential operational mode from anaerobic to aerobic conditions, with simultaneous addition of Fe(III) at the beginning of the aerobic phase.

**Here Fig. 5**

### *3.8 Performance and stability of the system at different pHs*

The decolorization and mineralization of MO at initial pH of 2.0 was always slightly higher

than that of pH 3.0, while at pH 4.0 a significant reduction of both values was observed (Fig. S8A and B). Higher pHs therefore unfavorably affected the system performance, in accordance with other electro-Fenton processes for the degradation of other organics [21,26,65,66].

After 10 consecutive operational cycles, the decolorization and mineralization of MO (Fig. 6a-b) remained unaffected at pH 2.0, while at pH of 3.0 MO mineralization was decreased by  $12.0 \pm 1.6\%$  (although the decolorization was unaffected) and at pH 4.0 a significant decrease of both MO decolorization ( $24.8 \pm 2.2\%$ ) and mineralization ( $59.4 \pm 1.8\%$ ) was observed. These results correlated well with the leaching of W and Mo from the cathodes, which reached 0.9 – 4.3 mg/L (W) and 1.5 – 6.3 mg/L (Mo) at pH 3.0, and 4.1 – 15.3 mg/L (W) and 7.6 – 20.5 mg/L (Mo) at pH 4.0 (Fig. 6C). The metals leaching at a high pH was caused by the significant increase in the effluent pH (Fig. 6D), because the solubilities of W and Mo deposits increases exponentially at higher pH values [14,27,31].

SEM, EDS and XRD further validated these observations. The morphology of the W and Mo deposits on the cathodes after 10 operational cycles was retained at an initial pH 2.0 (Fig. S9A and B), consistent with the stable operation (Fig. 6A and B). However, the characteristic mesh structure of the deposits after 10 operational cycles was destroyed at initial pH of 3.0 or 4.0 and instead only some irregular particles were observed on the cathodes (Fig. 9C – F). These results collectively demonstrated the higher stability of W and Mo catalytic species on the cathodes at more acidic initial pHs for the decolorization and mineralization of MO in the MFCs.

**Here Fig. 6**

#### **4. Conclusions**

Photo-assisted microbial fuel cells (MFCs) and Fenton assisted MFCs have been shown to be

efficient systems for azo dyes decolorization with simultaneous production of electricity, but the mineralization of the organic load in these systems is rarely achieved. This study demonstrated a novel strategy for efficient decolorization and mineralization of azo-dyes in wastewater in photo-assisted MFCs by sequential anaerobic - aerobic operation, in the presence of Fe(III), and W and Mo catalytic species. The reductive decolorization achieved during the anaerobic phase was followed by the further oxidation and mineralization of the reaction intermediates at the aerobic phase, augmented by hydroxyl radicals produced by both photoreduction of Fe(III), and electrochemical reduced Fe(II) and in-situ produced H<sub>2</sub>O<sub>2</sub> in electro-Fenton process. Such approach can be potentially extended to the oxidation of other organic contaminants in wastewater such as halogenated organic compounds and antibiotics, providing an alternative and environmentally benign approach for efficient remediation of azo dye contaminated water with simultaneous production of renewable energy.

## **Acknowledgments**

This Special Issue is dedicated to honor the retirement of Prof. César Pulgarin at the Swiss Federal Institute of Technology (EPFL, Switzerland), a key figure in the area of Catalytic Advanced Oxidation Processes. The authors gratefully acknowledge financial support from the National Natural Science Foundation of China (Nos. 51578104 and 21777017), and the Programme of Introducing Talents of Discipline to Universities (B13012).

## **References**

- [1] S. Khamparia, D.K. Jaspal, *Front. Environ. Sci. Eng.* 11 (2017) 8–18.
- [2] K. Solanki, S. Subramanian, S. Basu, *Bioresour. Technol.* 131 (2013) 564–571.
- [3] C.R. Holkar, A.J. Jadhav, D.V. Pinjari, N.M. Mahamuni, A.B. Pandit, *J. Environ. Manage.* 182 (2016) 351–366.
- [4] T. Pan, S. Ren, J. Guo, M. Xu, G. Sun, *Front. Environ. Sci. Eng.* 7 (2013) 185–190.
- [5] C. Su, W. Li, X. Liu, X. Huang, X. Yu, *Front. Environ. Sci. Eng.* 10 (2016) 37–45.
- [6] Y. Mu, K. Rabaey, R.A. Rozendal, Z. Yuan, J. Keller, *Environ. Sci. Technol.* 43 (2009)

5137–5143.

- [7] L. Liu, F. Li, C. Feng, X. Li, *Appl. Microbiol. Biotechnol.* 85 (2009) 175–183.
- [8] Q. Zhao, H. Yu, W. Zhang, F.T. Kabutey, J. Jiang, Y. Zhang, K. Wang, J. Ding, *Front. Environ. Sci. Eng.* 11 (2017) 13.
- [9] H. Ding, Y. Li, A. Lu, S. Jin, C. Quan, C. Wang, X. Wang, C. Zeng, Y. Yan, *Bioresour. Technol.* 101 (2010) 3500–3505.
- [10] Y. Hou, R. Zhang, Z. Yu, L. Huang, Y. Liu, Z. Zhou, *Bioresour. Technol.* 224 (2017) 63–68.
- [11] H. Han, C. Shi, L. Yuan, G. Sheng, *Appl. Energ.* 204 (2017) 382–389.
- [12] Y. Hou, Y. Gan, Z. Yu, X. Chen, L. Qian, B. Zhang, L. Huang, J. Huang, *J. Power Sources* 371 (2017) 26–34.
- [13] D. Robert, *Catal. Today* 122 (2007) 20–26.
- [14] Q. Wang, L. Huang, X. Quan, Q. Zhao, *J. Photochem. Photobiol. A* 357 (2018) 156–167.
- [15] E. Brillas, C.A. Martínez-Huitle, *Appl. Catal. B: Environ.* 166–167 (2015) 603–643.
- [16] S. Rtimi, C. Pulgarin, R. Sanjines, J. Kiwi, *Appl. Catal. B: Environ.* 162 (2015) 236–244.
- [17] Z. Li, X. Zhang, J. Lin, S. Han, L. Lei, *Bioresour. Technol.* 101 (2010) 4440–4445.
- [18] J. Sun, Z. Bi, B. Hou, Y. Cao, Y. Hu, *Water Res.* 45 (2011) 283–291.
- [19] F. Kong, A. Wang, H. Cheng, B. Liang, *Bioresour. Technol.* 151 (2014) 332–339.
- [20] S. Sultana, M.D. Khan, S. Sabir, K.M. Gani, M. Oves, M.Z. Khan, *New J. Chem.* 39 (2015) 9461–9470.
- [21] L. Fu, S. You, G. Zhang, F. Yang, X. Fang, *Chem. Eng. J.* 160 (2010) 164–169.
- [22] T. Ling, B. Huang, M. Zhao, Q. Yan, W. Shen, *Bioresour. Technol.* 203 (2016) 89–95.
- [23] C. Feng, F. Li, K. Sun, Y. Liu, L. Liu, X. Yue, H. Tong, *Bioresour. Technol.* 102 (2011) 1131–1136.
- [24] M.C. Ortega-Liébana, E. Sánchez-López, J. Hidalgo-Carrillo, A. Marinas, J.M. Marinas, F.J. Urbano, *Appl. Catal. B: Environ.* 127 (2012) 316–322.
- [25] H. Barndök, L. Blanco, D. Hermosilla, Á. Blanco, *Chem. Eng. J.* 284 (2016) 112–121.
- [26] C. Feng, F. Li, H. Liu, X. Lang, S. Fan, *Electrochim. Acta* 55 (2010) 2048–2054.
- [27] Q. Wang, L. Huang, X. Quan, Q. Zhao, *Electrochim. Acta* 247 (2017) 880–890.
- [28] L. Huang, T. Li, C. Liu, X. Quan, L. Chen, A. Wang, G. Chen, *Bioresour. Technol.* 128 (2013) 539–546.
- [29] Y. Zhang, L. Yu, D. Wu, L. Huang, P. Zhou, X. Quan, G. Chen, *J. Power Sources* 273 (2015) 1103–1113.
- [30] L. Huang, M. Li, Y. Pan, Y. Shi, X. Quan, G. Li Puma, *Chem. Eng. J.* 327 (2017) 584–596.
- [31] L. Huang, M. Li, Y. Pan, X. Quan, J. Yang, G. Li Puma, *J. Hazard. Mater.* 353 (2018) 348–359.
- [32] J. Gu, H. Yu, X. Quan, S. Chen, *Front. Environ. Sci. Eng.* 11 (2017) 13.
- [33] W. Guo, Y. Cui, H. Song, J. Sun, *Bioprocess Biosyst. Eng.* 37 (2014) 1749–1758.
- [34] R. Liu, G. Sheng, M. Sun, G. Zang, W. Li, Z. Tong, F. Dong, M. Lam, H. Yu, *Appl. Microbiol. Biotechnol.* 89 (2011) 201–208.
- [35] C. Zhou, C. Lai, D. Huang, G. Zeng, C. Zhang, M. Cheng, L. Hu, J. Wan, W. Xiong, M. Wen, X. Wen, L. Qin, *Appl. Catal. B: Environ.* 220 (2018) 202–210.
- [36] C. Zhou, C. Lai, P. Xu, G. Zeng, D. Huang, C. Zhang, M. Cheng, L. Hu, J. Wan, Y. Liu, W. Xiong, Y. Deng, M. Wen, *ACS Sustainable Chem. Eng.* 6 (2018) 4174–4184.
- [37] X. Yang, F. Qian, Y. Wang, M. Li, J. Lu, Y. Li, M. Bao, *Appl. Catal. B: Environ.* 200 (2017) 283–296.

- [38] T. Chen, W. Gu, G. Li, Q. Wang, P. Liang, X. Zhang, X. Huang, *Front. Environ. Sci. Eng.* 12 (2018) 6–11.
- [39] Y. Gao, J. Lin, Q. Zhang, H. Yu, F. Ding, B. Xu, Y. Sun, Z. Xu, *Appl. Catal. B: Environ.* 224 (2018) 586–593.
- [40] R. Cai, B. Zhang, J. Shi, M. Li, Z. He, *ACS Sustain. Chem. Eng.* 5 (2017) 7690–7699.
- [41] B. Zhang, S. Zou, R. Cai, M. Li, Z. He, *Appl. Catal. B: Environ.* 224 (2018) 383–393.
- [42] M. M. Ballesteros Martín, J. A. Sánchez Pérez, J. L. García Sánchez, J. L. Casas López, S. Malato Rodríguez, *Water Res.* 43 (2009) 3838–3848.
- [43] P. Salgado, V. Melin, M. Albornoz, H. Mansilla, G. Vidal, D. Contreras, *Appl. Catal. B: Environ.* 226 (2018) 93–102.
- [44] J. Fan, Y.H. Guo, J.J. Wang, M.H. Fan, *J. Hazard. Mater.* 166 (2009) 904–910.
- [45] G. Boczkaj and A. Fernandes, *Chem. Eng. J.* 320 (2017) 608–633.
- [46] M. Punzi, A. Anbalagan, R.A. Börner a, B.M. Svensson, M. Jonstrup, B. Mattiasson, *Chem. Eng. J.* 270 (2015) 290–299.
- [47] L. Huang, X. Yang, X. Quan, J. Chen, F. Yang, *J. Chem. Technol. Biotechnol.* 85 (2010) 621–627.
- [48] State Environment Protection Administration, *the Water and Wastewater Monitoring Methods*, fourth ed., China Environmental Science Press, Beijing, 2002.
- [49] S. Zou, Z. He, *Water Res.* 131 (2018) 62–73.
- [50] A. Jain, Z. He, *Front. Environ. Sci. Eng.* 12 (2018) 1.
- [51] S. Ren, M. Li, J. Sun, Y. Bian, K. Zuo, X. Zhang, P. Liang, X. Huang, *Front. Environ. Sci. Eng.* 11 (2017) 17.
- [52] S.M.D.A.G. Ulson, K.A.S. Bonilla, A.A.U. de Souza, *J. Hazard. Mater.* 179 (2010) 35–42.
- [53] A. Arfaoui, S. Touihri, A. Mhamdia, A. Labidi, T. Manoubi, *Appl. Surf. Sci.* 357 (2015) 1089–1096.
- [54] S. Li, H. Hou, Z. Huang, H. Liao, X. Qiu, X. Ji, *Electrochim. Acta* 245 (2017) 949–956.
- [55] M. Cheng, G. Zeng, D. Huang, C. Lai, Y. Liu, C. Zhang, J. Wan, L. Hu, C. Zhou, W. Xiong, *Water Res.* 138 (2018) 7–18.
- [56] H. Dong, C. Sans, W. Li, Z. Qiang, *Sep. Purif. Technol.* 171 (2016) 144–150.
- [57] D. He, Y. Chen, Y. Situ, L. Zhong, H. Huang, *Appl. Surf. Sci.* 425 (2017) 862–872.
- [58] Z. Wang, B. Zhang, A. Borthwick, C. Feng, J. Ni, *Chem. Eng. J.* 280 (2015) 99–105.
- [59] S.C. Yan, Z.S. Li, Z.G. Zou, *Langmuir* 26 (2010) 3894–3901.
- [60] G. Ferro, A. Fiorentino, M. Castro Alferéz, M.I. Polo-López, L. Rizzo, P. Fernández-Ibáñez, *Appl. Catal. B: Environ.* 178 (2015) 65–73.
- [61] S. Giannakis, M.I. Polo-López, D. Spuhler, J.A. Sánchez Pérez, P. Fernández-Ibáñez, C. Pulgarin, *Appl. Catal. B: Environ.* 198 (2016) 431–446.
- [62] P. Cai, X. Xiao, Y. He, W. Li, J. Chu, C. Wu, M. He, Z. Zhang, G. Sheng, M. Lam, F. Xu, H. Yu, *Appl. Microbiol. Biotechnol.* 93 (2012) 1769–1776.
- [63] K.I. Konstantinou, T.A. Albanis, *Appl. Catal. B: Environ.* 49 (2004) 1–14.
- [64] L.G. Devi, S.G. Kumar, K.M. Reddy, C. Munikrishna, *J. Hazard. Mater.* 164 (2009) 459–467.
- [65] X. Liu, W. Li, H. Yu, *Chem. Soc. Rev.* 43 (2014) 7718 – 7745.
- [66] C. He, Z. Mu, H. Yang, Y. Wang, Y. Mu, H. Yu, *Chemosphere* 140 (2015) 12 – 17.



**Fig. 1** Comparison of (A) MO decolorization, (B) MO mineralization, (C) circuit current, and (D) power output in MFCs with or without (control) W and Mo deposits under fully anaerobic conditions and in the presence or absence (control) of light irradiation.

**Fig. 2** Comparison of (A) MO decolorization, (B) MO mineralization, (C) circuit current, and (D) power output in MFCs with or without (control) W and Mo deposits under fully aerobic conditions and in the presence or absence (control) of light irradiation or Fe(III) (5 mg/L).

**Fig. 3** (A) MO decolorization in the presence of light irradiation with addition of ammonium oxalate (AO), isopropanol (IP) or benzoquinone (BQ), and the corresponding UV-vis absorption spectra of the effluents in the absence (B) or presence of (C) either O<sub>2</sub>, or (D) both O<sub>2</sub> and Fe(III).

**Fig. 4** (A) MO mineralization, and (B) percentage of Fe(III) in catholyte as a function of time in the MFCs with a shift from anaerobic (20 min) to aerobic (100 min) conditions with simultaneous addition of various dosages of Fe(III).

**Fig. 5** Comparison of intermediates of MO decolorization and mineralization in the catholyte effluents in the absence (A) or presence (B) of O<sub>2</sub>, (C) co-presence of O<sub>2</sub> and Fe(III), or (D) a shift from anaerobic to aerobic conditions with simultaneous addition of 10 mg/L Fe(III).

**Fig. 6** Comparison of (A) MO decolorization, (B) MO mineralization, (C) leached W and Mo, and (D) effluent pH as a function of number of cycle at an initial pH of 2.0, 3.0 or 4.0 and under sequential anaerobic - aerobic operation with simultaneous addition of 10 mg/L Fe(III).

Figure 1  
[Click here to download high resolution image](#)

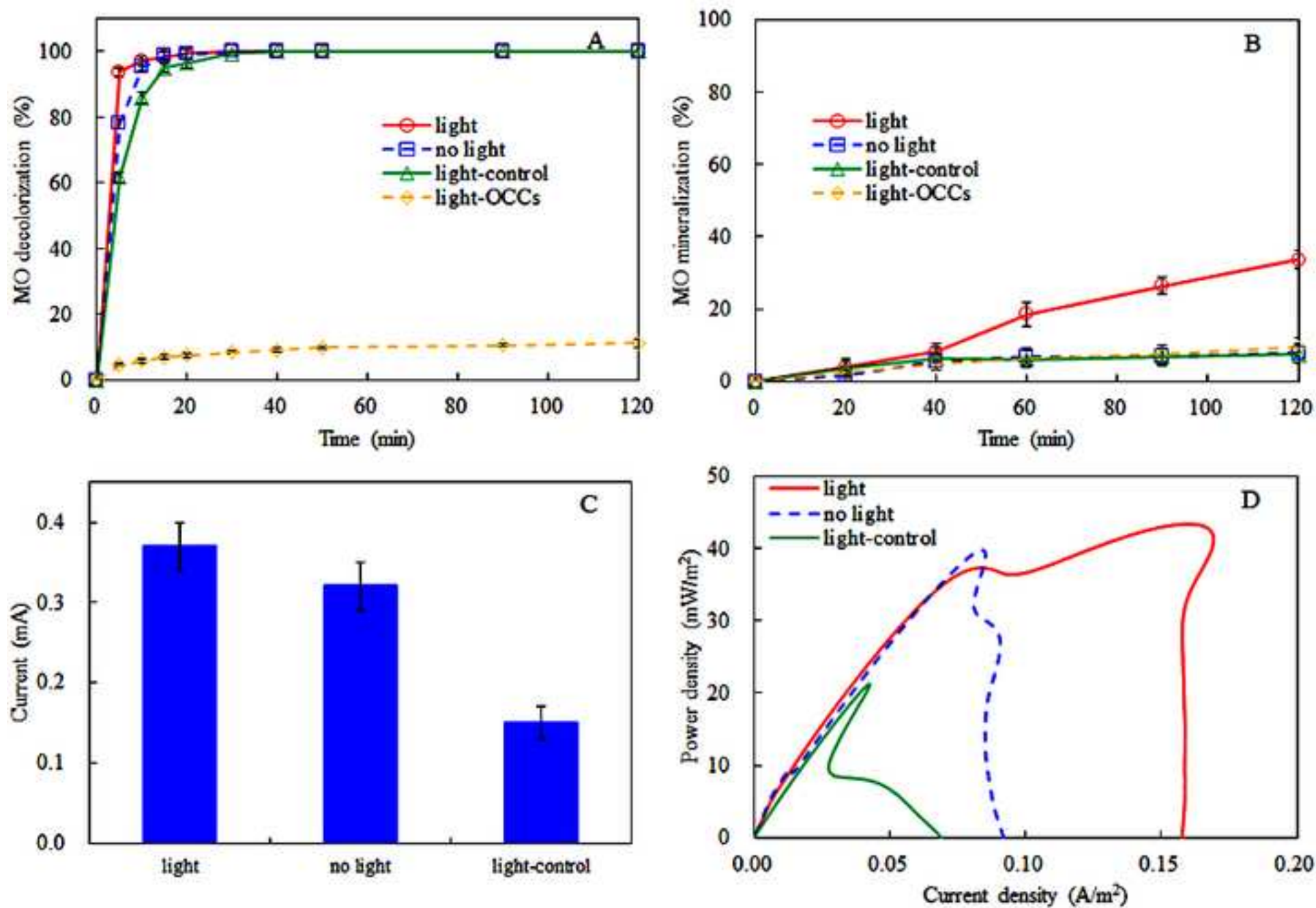


Figure 2  
[Click here to download high resolution image](#)

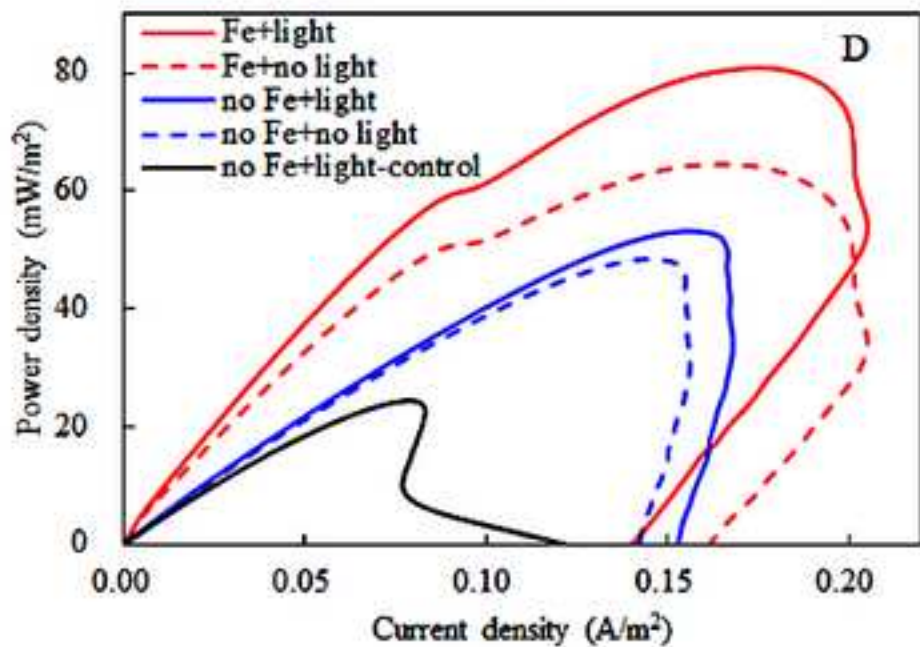
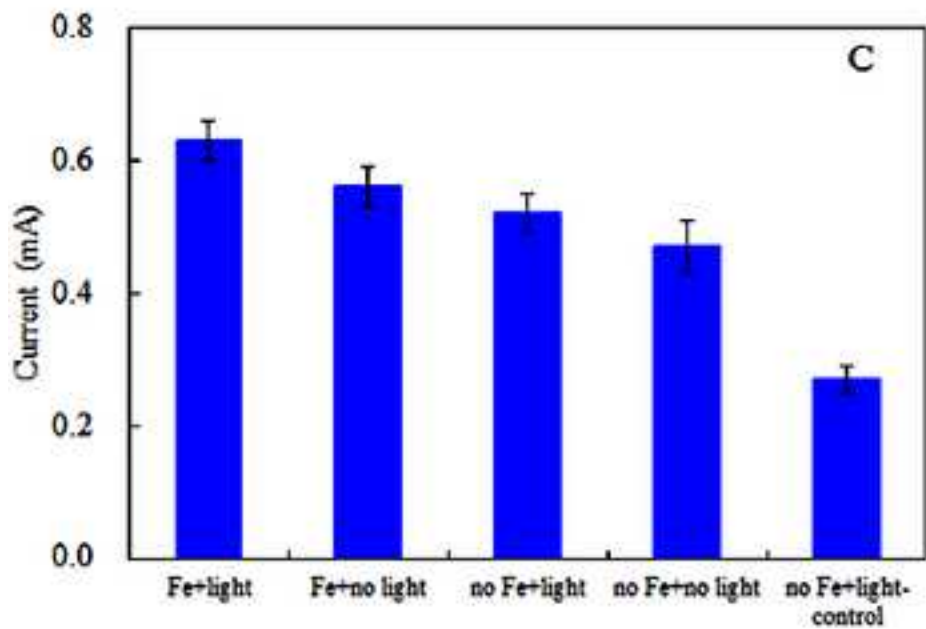
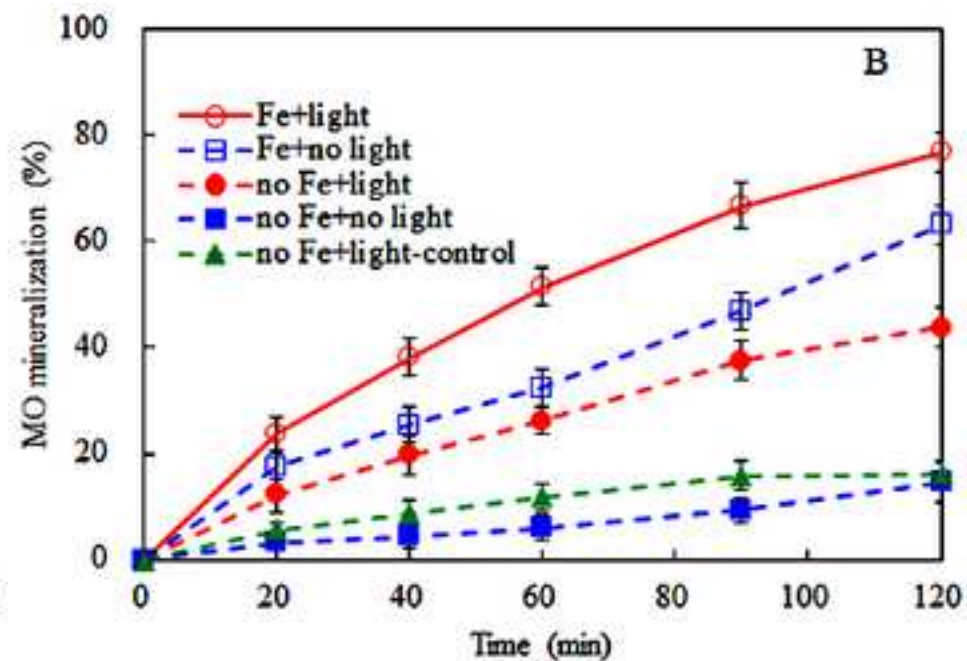
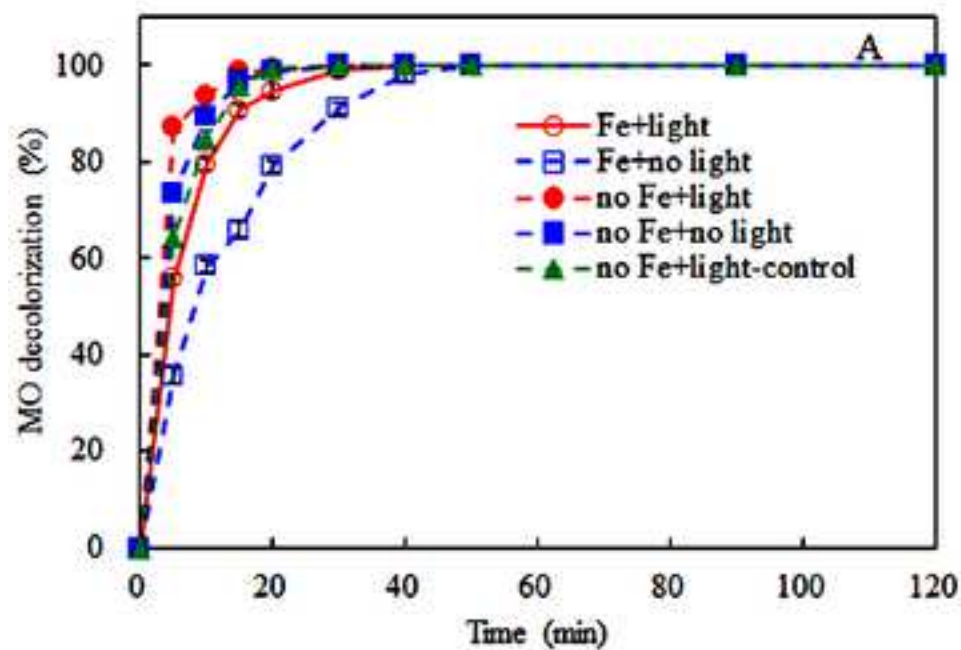


Figure 3  
[Click here to download high resolution image](#)

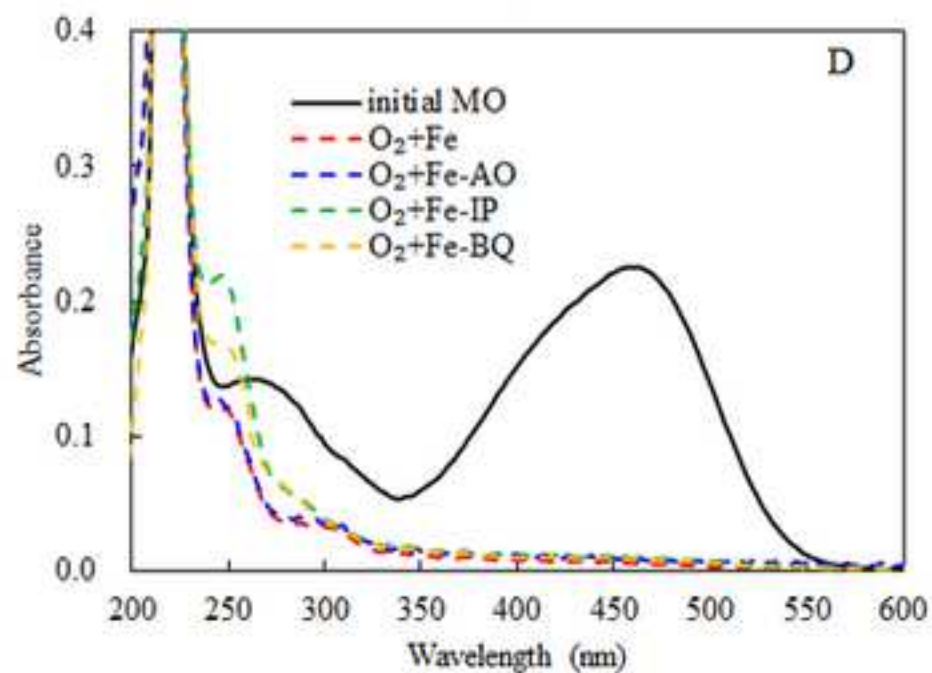
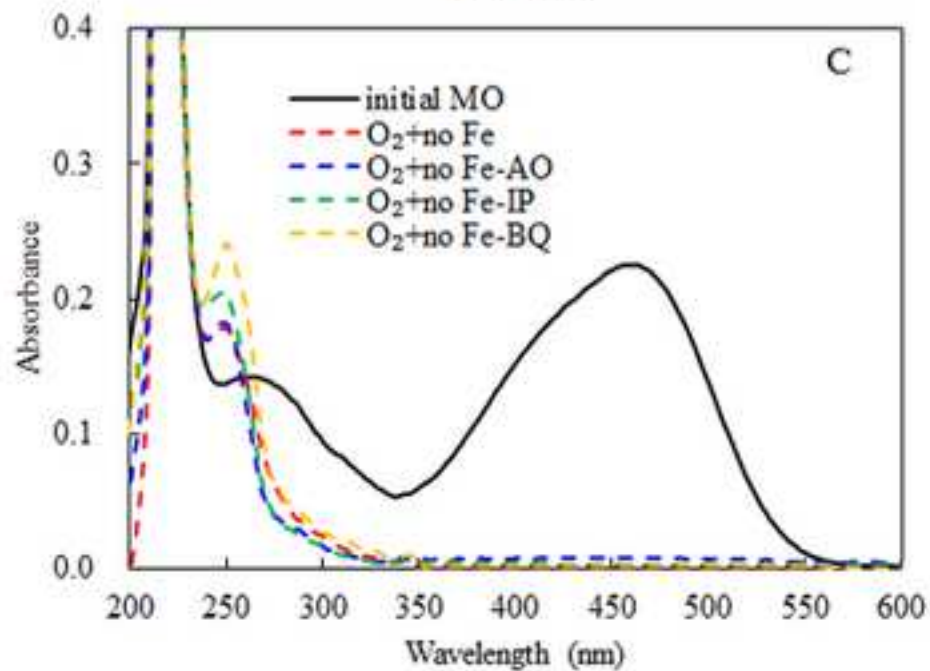
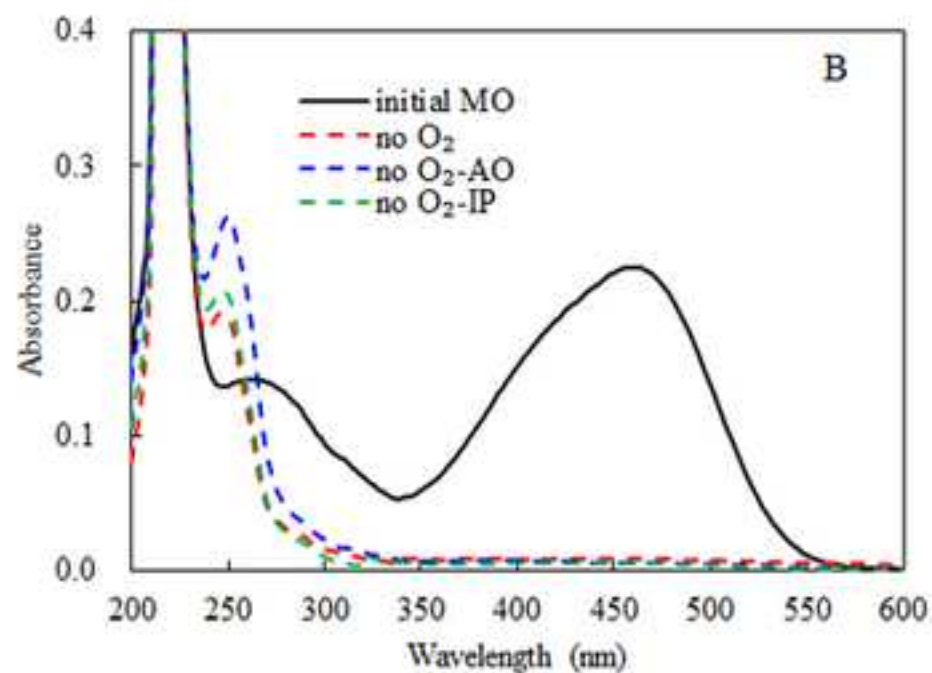
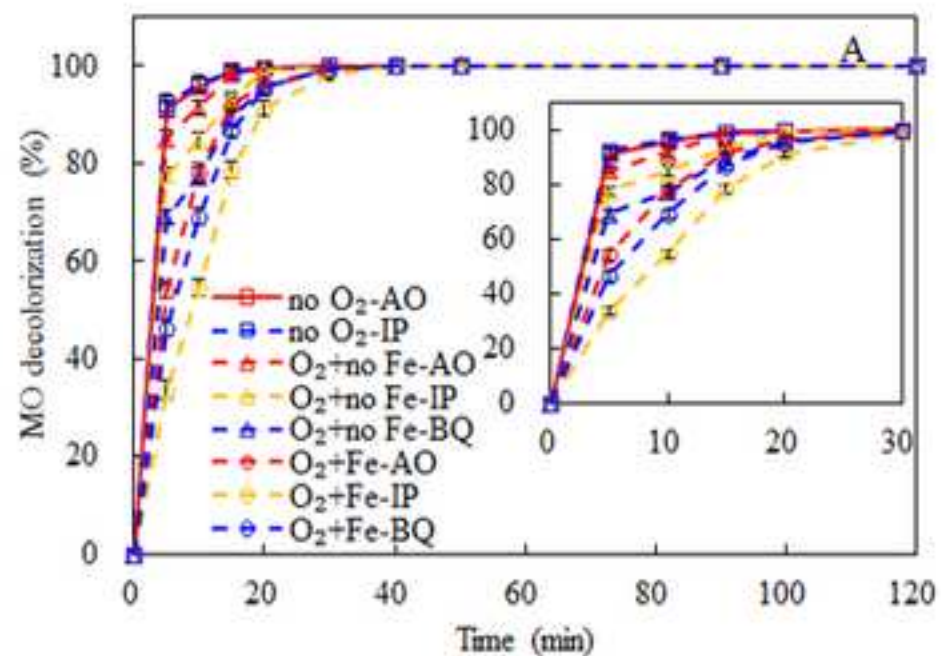


Figure 4  
[Click here to download high resolution image](#)

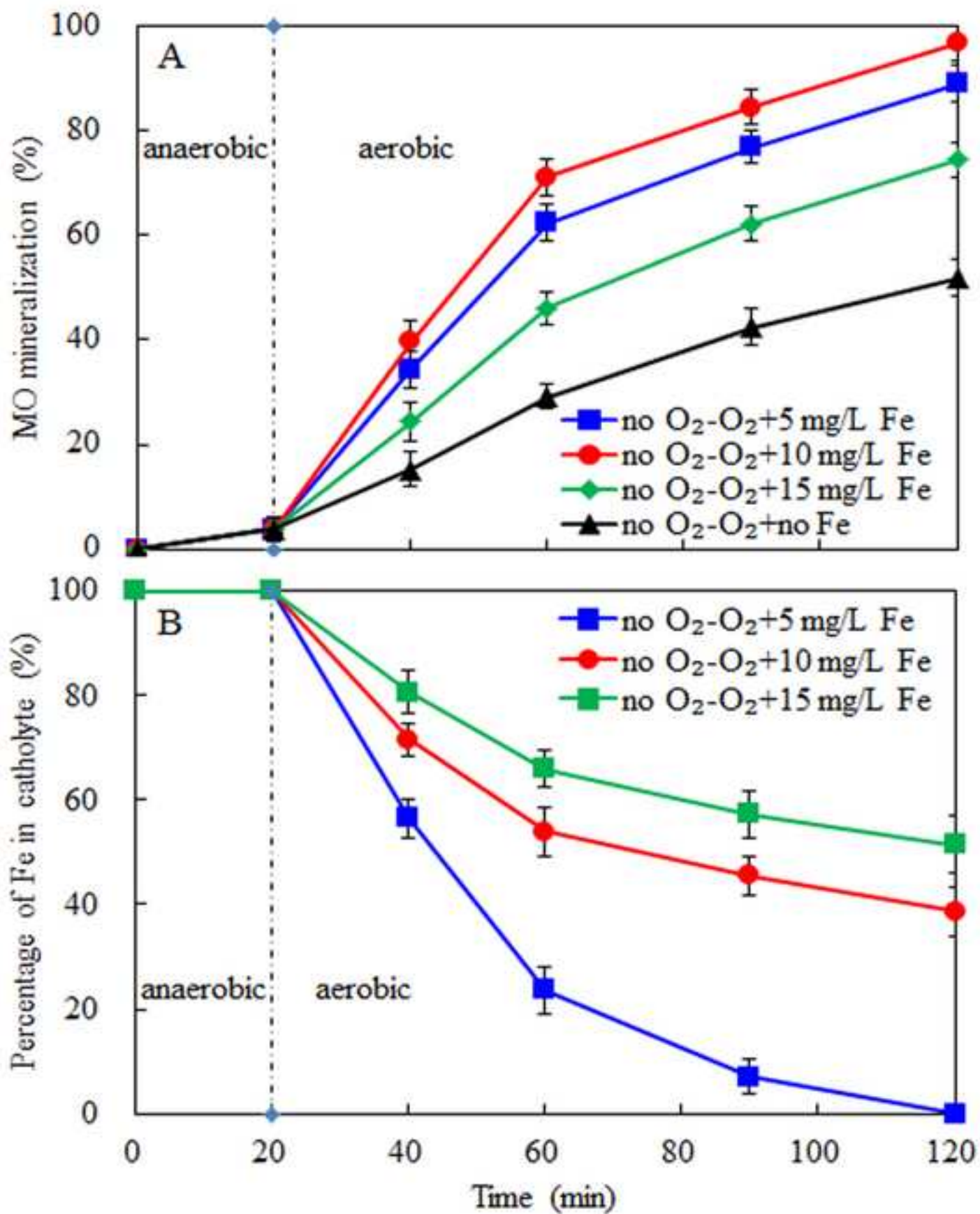


Figure 5  
[Click here to download high resolution image](#)

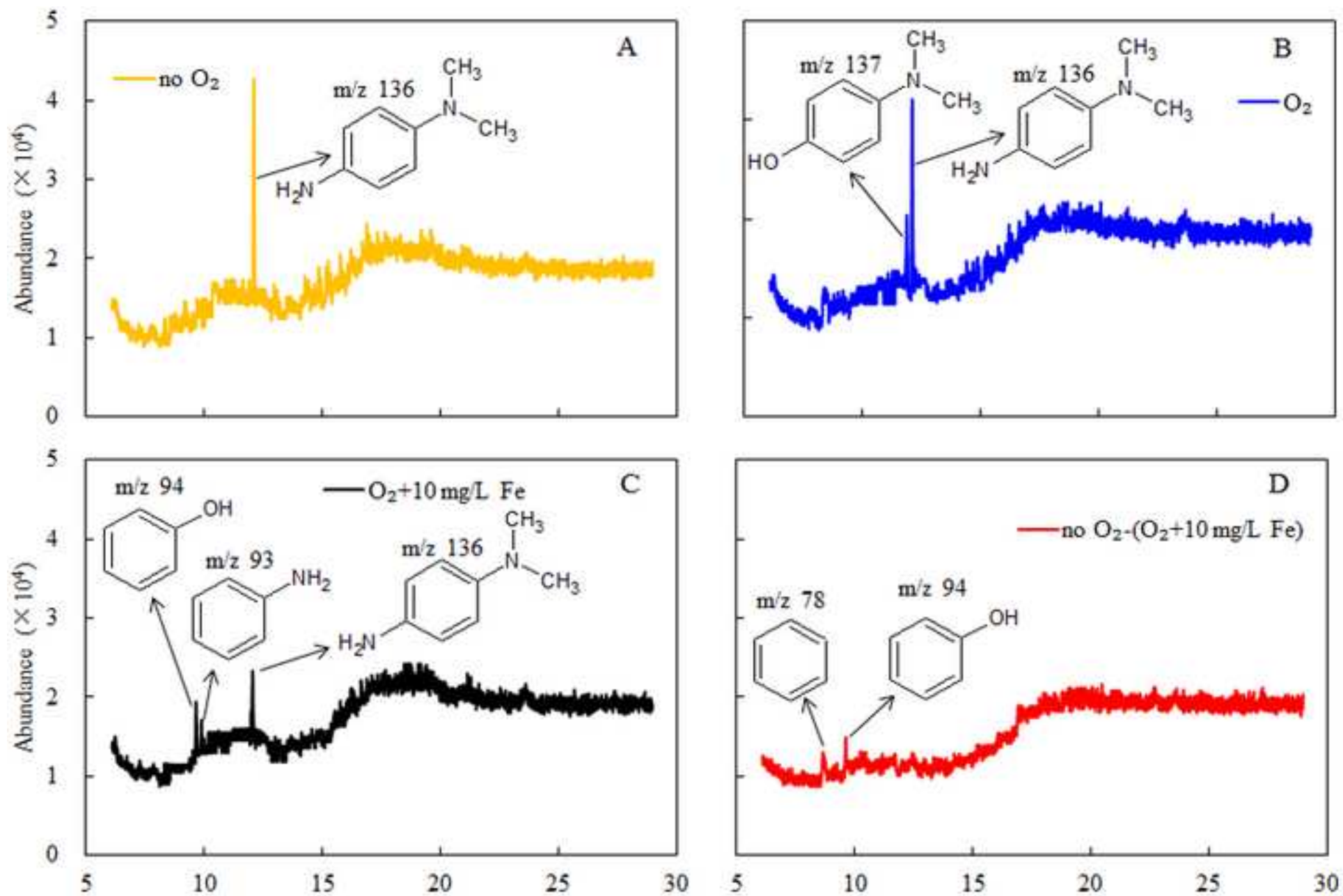
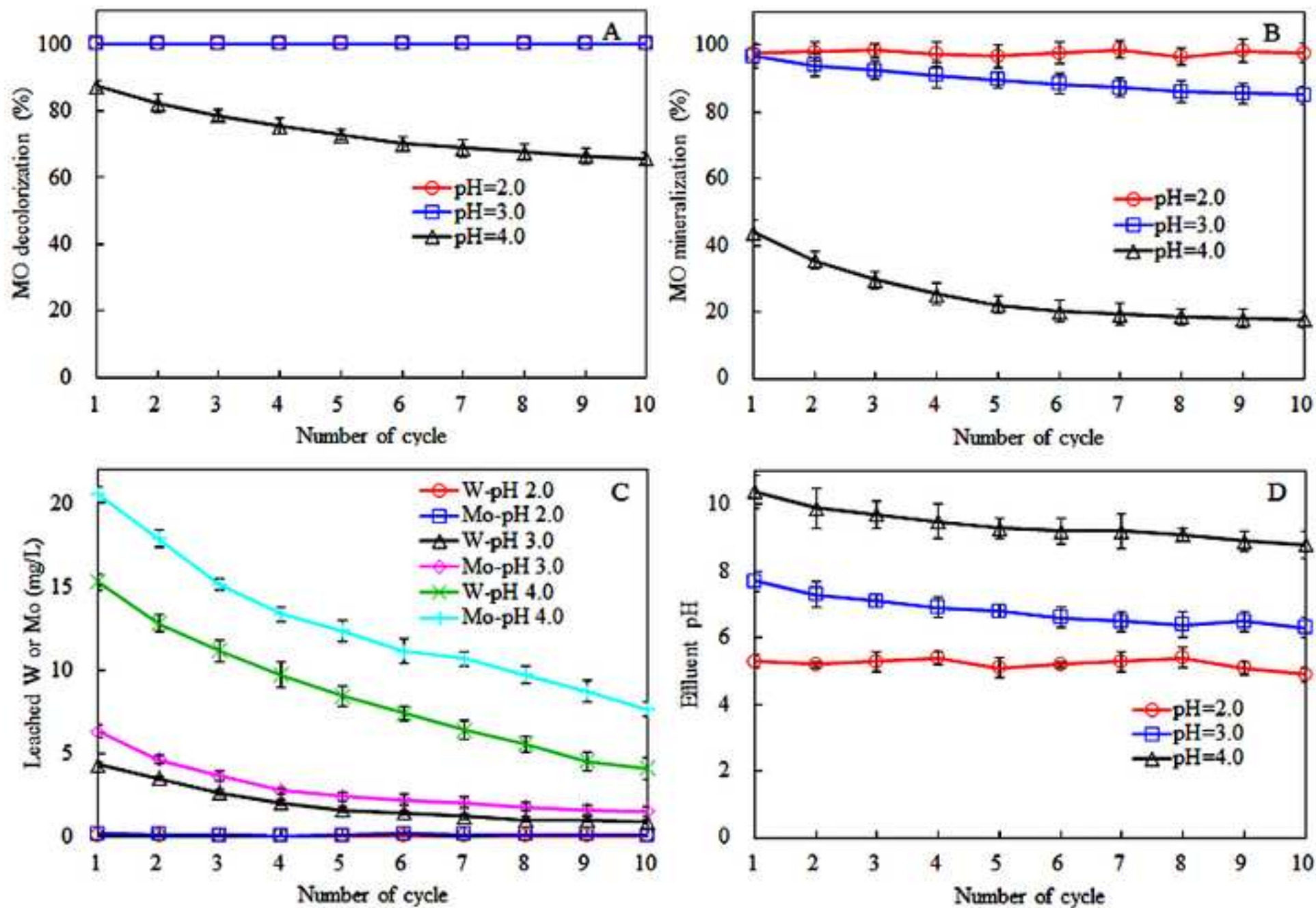
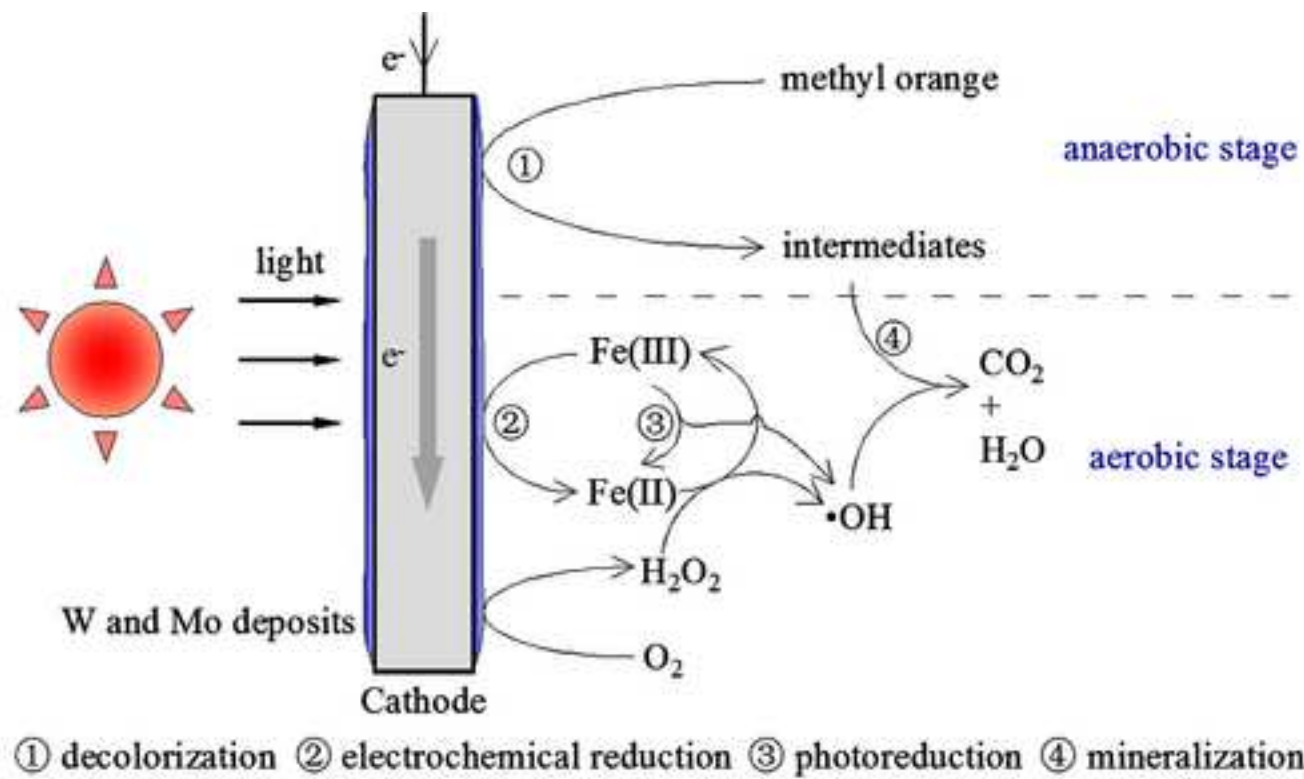


Figure 6  
[Click here to download high resolution image](#)







## Highlights

- Azo dye MO mineralization intensified in photo-assisted microbial fuel cells;
- W and Mo deposited on the cathodes favors the reductive decolorization of azo dyes;
- Sequential anaerobic-aerobic operation with Fe(III) is the most effective process;
- Complete mineralization of azo dye MO achieved under optimized conditions.

**Supplementary Material**

[Click here to download Supplementary Material: Supplementary Material.doc](#)